Catalysis Today 175 (2011) 293–298

Contents lists available at ScienceDirect

Catalysis Today

journal homepage: www.elsevier.com/locate/cattod

Synthesis of $TiO_2/SiO_2@Fe_3O_4$ magnetic microspheres and their properties of photocatalytic degradation dyestuff

Hongfei Liu, Zhigang Jia, Shengfu Ji*, Yuanyuan Zheng, Ming Li, Hao Yang

State Key Laboratory of Chemical Resource Engineering, Beijing University of Chemical Technology, Beijing 100029, PR China

ARTICLE INFO

Article history:
Received 30 October 2010
Received in revised form 15 April 2011
Accepted 23 April 2011
Available online 1 June 2011

Keywords:
$TiO_2/SiO_2@Fe_3O_4$
Magnetic microspheres
Photocatalyst
Rhodamine
Degradation

ABSTRACT

The $TiO_2/SiO_2@Fe_3O_4$ photocatalysts were synthesized via two steps. First, the $SiO_2@Fe_3O_4$ particles were synthesized using Fe_3O_4 as the core and tetraethoxysilane (TEOS) as silica source. Second, the anatase TiO_2 was coated on the $SiO_2@Fe_3O_4$ particle surface using tetrabutyl titanate (TBOT) as titanium source. The synthesized samples were characterized by X-ray diffraction (XRD), transmission electron microscopy (TEM), N_2 adsorption–desorption techniques and vibration sample magnetometer (VSM). The catalytic activity of $TiO_2/SiO_2@Fe_3O_4$ catalysts for the photocatalytic degradation of Rhodamine (RhB) was evaluated under ultraviolet (UV) irradiation. The results indicated that the mean size of the $6\%SiO_2@Fe_3O_4$ particles was about 75–80 nm and thickness of the homogeneous SiO_2 layer was about 2–3 nm. The diameter of $50\%TiO_2/6\%SiO_2@Fe_3O_4$ microspheres was about 100 nm and thickness of the homogeneous anatase TiO_2 layer was about 8–10 nm. The saturation magnetization and specific surface area of $50\%TiO_2/6\%SiO_2@Fe_3O_4$ catalysts were 48.6 emu/g and 495.3 m^2/g, respectively. The $50\%TiO_2/6\%SiO_2@Fe_3O_4$ microspheres exhibited the best photocatalytic performance. The conversion of RhB achieved up to 98.1% after 60 min UV irradiation, and the photocatalytic reaction apparent rate constant k_a was 0.05288 min^{-1}. After used for 8 times, it also maintained high degradation rate and catalyst recovery.

1. Introduction

Wastewater produced by chemical industry, textile industry and leather manufacturing, often contains considerable amounts of organic dyes pollutants, which will cause irreparable damage to natural environment and human health. Therefore, it appears especially significant to treat organic dyes wastewater. Photocatalytic oxidation using photocatalyst is an effective treatment method for organic dyes wastewater. Nanosized TiO_2, owing to its favorable characteristics such as low cost, good chemical stability, high photocatalytic activity, nontoxic nature, and wide range of application [1–5], is one of the most widely used photocatalysts being studied. However, the industrial application of nanometer TiO_2 was still limited mainly due to easy loss and difficult recovery. Nanocrystalline TiO_2 immobilized on supporting materials such as glass, sand, or zeolite can improve the separation efficiency [6,7], but it was difficult to maintain a high photocatalytic activity due to the decrease of specific surface after immobilization [8].

Magnetic separation provides a very convenient approach for removing and recycling magnetic particles by external magnetic field. Recently, the incorporation of magnetic components into TiO_2 nanoparticle-based catalysts attracted significant attention [9,10]. He et al. [11] used the $Ti(SO_4)_2$ as titanium sources, obtained the core-shell structure $TiO_2@Fe_3O_4$ catalysts by homogeneous precipitation. These catalysts had good photocatalytic activity and recycling performance, but preparation process was relatively complex. Xuan et al. [12] had synthesized Fe_3O_4/TiO_2 hollow spheres through a poly(styrene-acrylic acid) (PSA) template method, the catalyst exhibited good photocatalytic activity under UV light irradiation and could be recycled six times by magnetic separation without major loss of activity. Gao et al. [13] used the tetrabutyl titanate as titanium sources, prepared the $TiO_2@\gamma\text{-}Fe_2O_3$ particles, which exhibited good degradation activity for acridine dyes, but the magnetic particles were sensitive and unstable, especially under acidic conditions. Furthermore, the formation of anatase TiO_2 usually involves high-temperature annealing; magnetic materials, such as $\gamma\text{-}Fe_2O_3$ and Fe_3O_4 may rapidly transform to the antiferromagnetic $\alpha\text{-}Fe_2O_3$ and lose the magnetic response during the heat treatment process. Worse still, the TiO_2 layer can cause interaction with $\gamma\text{-}Fe_2O_3$ and Fe_3O_4, reducing the photocatalytic activity [14–16].

In this study, the core-shell structured $TiO_2/SiO_2@Fe_3O_4$ microsphere catalysts, added a SiO_2 layer between the Fe_3O_4 core and the outer layer of TiO_2, were prepared by two steps. The SiO_2 layer can effectively not only reduce the interaction between magnetic core and the out layer of TiO_2 but also stabilize the magnetic core.

* Corresponding author. Tel.: +86 10 64419619; fax: +86 10 64419619.
E-mail address: jisf@mail.buct.edu.cn (S. Ji).

0920-5861/$ – see front matter © 2011 Elsevier B.V. All rights reserved.
doi:10.1016/j.cattod.2011.04.042

The structure of samples was characterized by X-ray diffraction, transmission electron microscopy, N_2 adsorption–desorption techniques and vibration sample magnetometer. The photocatalytic activity for the photocatalytic degradation of Rhodamine (RhB) was measured; the influences of initial concentration of RhB solution and dosage of catalyst on the performance of the catalysts were investigated respectively. Meanwhile, the reusable activity was studied.

2. Experimental

2.1. Preparation of samples

2.1.1. Synthesis of Fe_3O_4

The magnetic particles were prepared through a solvothermal reaction [17]. Briefly, 2.7 g of $FeCl_3{\cdot}6H_2O$ and 7.2 g of sodium acetate were dissolved in appropriate of ethylene glycol under stirring. The obtained homogeneous yellow solution was transferred to a Teflon-lined stainless-steel autoclave. The autoclave was sealed and heated at 200 °C under 400 rpm speed. After reaction for 8 h, the autoclave was naturally cooled to room temperature. The obtained black magnetite particles were separated with a permanent magnet, washed with ethanol for 6 times, and dried in vacuum at 50 °C for 24 h.

2.1.2. Synthesis of SiO_2@Fe_3O_4

0.1 g of obtained Fe_3O_4 particles was dispersed into the mixture solution of 80 mL of ethanol, 20 mL of deioned water, and 1.0 mL of concentrated ammonia aqueous solution (28 wt%). After this, the mixture solution was homogenized by ultrasonication for 30 min to form a uniform dispersion. Subsequently, a certain amount of tetraethoxysilane (TEOS) was added dropwise into the solution with vigorous stirring. After stirred at room temperature for 6 h, the product was separated with a permanent magnet, washed with deionized water for 3 times, and dried in vacuum at 50 °C for 12 h. A series of SiO_2@Fe_3O_4 particles were prepared with 1–9% SiO_2 content.

2.1.3. Synthesis of TiO_2/SiO_2@Fe_3O_4

Typically, the above obtained SiO_2@Fe_3O_4 particles were dispersed in 40 mL of ethanol and homogenized by ultrasonication for 30 min. After that, an appropriate amount of tetrabutyl titanate (TBOT) and glacial acetic acid (volume ratio 5:1) were orderly introduced to the solution under vigorous mechanical stirring. After stirred at room temperature for 4 h, 15 mL of ethanol and 3 mL of deionized water were added to the system, and then the solution was heated at 45 °C. The final product was dried in vacuum at 50 °C and calcined in nitrogen protection at 500 °C for 3 h. A series of TiO_2/SiO_2@Fe_3O_4 particles were prepared with 10–67% TiO_2 content.

2.2. Characterization of samples

The X-ray diffraction (XRD) patterns were recorded using a D/Max 2500 VB2+/PC diffractometer with Cu Kα irradiation (λ = 1.5418 Å) at 200 kV and 50 mA in the range of 2θ value between 10° and 90°. Transmission electron microscopy (TEM) observation was performed on a JEOL (JEM 2100) transmission emission microscope operated at a 200 kV accelerating voltage. Magnetic properties of the samples were measured using a vibration sample magnetometer (VSM; Lake Shore Model 7400) under magnetic fields up to 20 kOe. The N_2 adsorption–desorption analysis was tested on a ASAP 2020M automatic specific surface area and aperture analyzer. The samples were pretreated at 300 °C for 4 h and the specific surface area of samples determined using the Brunauer–Emmett–Teller (BET) method. The pore volume and pore size distribution were derived from the desorption profiles of the isotherms using the Barrett–Joyner–Halanda (BJH) method.

2.3. Photocatalytic performance measurement

The catalytic reaction was carried out on a self-made continuous stirred liquid–solid photocatalytic reactor. The temperature of the reaction was maintained at room temperature by circulating water. A 500 W high-pressure mercury lamp (the peak wavelength was 365 nm) placed 20 cm above the reaction suspension, was used as the UV radiation source. The aqueous suspension, prepared with amount of catalysts and 200 mL of RhB solution in different concentrations, was stirred in the dark for 30 min to ensure that the dye molecules were adsorbed to saturation on the catalysts. The lamp preheated 5 min and started the timer. The water samples were collected for analysis every 15 min. The reaction suspension was taken regularly and illuminated over 60 min. The water samples taken from the magnetic separation, were determined the absorbency in the maximum absorption wavelength with UV–vis spectrophotometer (TU-1901, Beijing Burkinje general instrument Co. Ltd.). Subsequently, we calculated the RhB concentration change (C/C_0) and the conversion of RhB ($(C_0 - C)/C_0$), plotted the relationship curves of C/C_0 and $(C_0 - C)/C_0$ vs. irradiation time, and fitted the photocatalytic reaction kinetics equation $\ln C_0/C = k_a t$, k_a was photocatalytic reaction apparent rate constant, C_0 and C were the initial and actual concentration of RhB [18]. The used catalysts were separated with a permanent magnet, washed with ethanol for 6 times, dried in vacuum at 50 °C for 24 h, and then used for investigating the recyclability of catalysts at the same reaction system.

3. Results and discussion

3.1. XRD

The large-angle XRD patterns of all samples are shown in Fig. 1. It can be seen that all samples obtained have highly crystalline cubic spinel structure agreed well with the standard Fe_3O_4 (cubic phase) XRD spectrum (PDF #88-0866). From the Fig. 1b–e, the XRD patterns of SiO_2@Fe_3O_4 prepared show a obviously broad

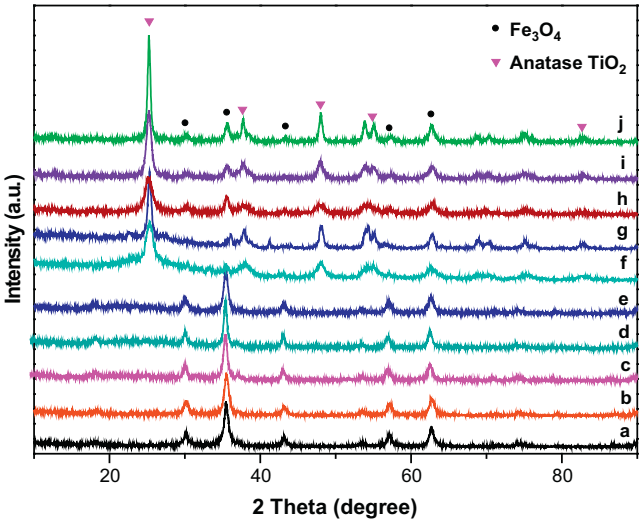

Fig. 1. The large-angle XRD patterns of samples: (a) Fe_3O_4; (b) 1%SiO_2@Fe_3O_4; (c) 3%SiO_2@Fe_3O_4; (d) 6%SiO_2@Fe_3O_4; (e) 9%SiO_2@Fe_3O_4; (f) 10%TiO_2/6%SiO_2@Fe_3O_4; (g) 20%TiO_2/6%SiO_2@Fe_3O_4; (h) 33%TiO_2/6%SiO_2@Fe_3O_4; (i) 50%TiO_2/6%SiO_2@Fe_3O_4; (j) 67%TiO_2/6%SiO_2@Fe_3O_4.

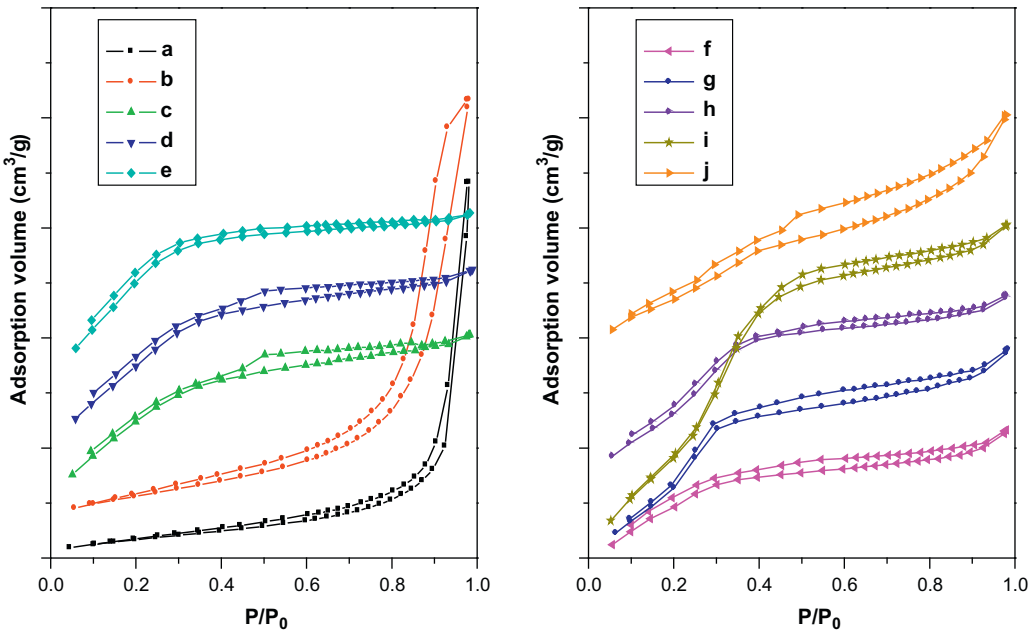

Fig. 2. N_2 adsorption–desorption isotherms of samples: (a) Fe_3O_4; (b) 1%SiO_2@Fe_3O_4; (c) 3%SiO_2@Fe_3O_4; (d) 6%SiO_2@Fe_3O_4; (e) 9%SiO_2@Fe_3O_4; (f) 10%TiO_2/6%SiO_2@Fe_3O_4; (g) 20%TiO_2/6%SiO_2@Fe_3O_4; (h) 33%TiO_2/6%SiO_2@Fe_3O_4; (i) 50%TiO_2/6%SiO_2@Fe_3O_4; (j) 67%TiO_2/6%SiO_2@Fe_3O_4.

peak at $2\theta = 15–25^\circ$, generally be considered as the peak of amorphous silica [17]. The enhancement of intensity revealed that the thickness of amorphous silica increased. From the Fig. 1f–j, all TiO_2/SiO_2@Fe_3O_4 samples obtained have the characteristic peaks of anatase TiO_2 agreed well with the standard anatase TiO_2 XRD spectrum (PDF #71-1166), and the peaks of Fe_3O_4 are weakened. It revealed that Fe_3O_4 core had no obvious changes after coated with SiO_2 and TiO_2. There are enhancements in the diffraction intensity of anatase TiO_2 as the TiO_2 content increasing from 10% to 67%.

3.2. BET

The N_2 adsorption–desorption isotherms of all samples are shown in Fig. 2. It was found that a linear increase in the amount of adsorbed nitrogen at a low relative pressure. All isotherms of SiO_2@Fe_3O_4 (Fig. 2c–e) except 1%SiO_2@Fe_3O_4 sample, were the type I patterns with distinct H4 hysteretic loops. The TiO_2/SiO_2@Fe_3O_4 samples exhibited combination of type I and IV patterns with distinct H2 and H4 hysteretic loops, which demonstrated the existences of micro- and mesopores according to the IUPAC classification. It was these bimodal pores structure that allowed rapid diffusion of various reactants and products during the photocatalytic reaction and enhanced the rate of the photocatalytic reaction [18]. Textural and structural characteristics of the samples are listed in Table 1. From Table 1, the BET surface area of the Fe_3O_4 particles is 40.9 m^2/g and the BJH pore volume is 0.27 cm^3/g. With the SiO_2 content increasing from 1% to 6%, the BET surface area of the SiO_2@Fe_3O_4 particles are obviously increased, but the BJH pore volume and average pore size are decreased. The BET surface area and BJH pore volume of 6%SiO_2@Fe_3O_4 particles are 315.5 m^2/g and 0.16 cm^3/g, respectively. When the SiO_2 content reaches to 9%, the BET surface area decrease to 266.0 m^2/g. The SiO_2 content keeps in 6%, the BET surface area and BJH pore volume of TiO_2/SiO_2@Fe_3O_4 samples are obviously increased with the TiO_2 content increasing from 10% to 50% [15,16]. The 50%TiO_2/6%SiO_2@Fe_3O_4 microspheres have the biggest BET surface area and BJH pore volume, which are 495.3 m^2/g and 0.54 cm^3/g, respectively. The increases of the specific surface and pore volume correspondingly augment dye absorption quantity and ultraviolet absorption area, which can effectively improve the photocatalytic efficiency. The cause for the BET surface area reduced at 67% TiO_2 content is probably the aggregated of microspheres.

3.3. TEM and VSM

Fig. 3 shows the TEM images of (a), (b) Fe_3O_4 and (c) 6%SiO_2@Fe_3O_4 as well as (d) 50%TiO_2/6%SiO_2@Fe_3O_4. It can be found that the Fe_3O_4 particles, composed of several small Fe_3O_4 nanoparticles (about 20 nm), are spherical, and the average diameter of the spherical particles is about 70 nm (Fig. 3a). The structural details are revealed in Fig. 3b, it can be observed clearly that the small Fe_3O_4 nanoparticles have aggregated into Fe_3O_4 spherical particles [19], and the parallel lattice fringes across almost all the primary nanoparticles are clearly visible. The upper right Fourier transform image gives the characteristic spot pattern of a Fe_3O_4 nanocrystal. The mean diameter is about 75–80 nm for the 6%SiO_2@Fe_3O_4 particles because of surface coated of silica on the shell, and the average thickness of the homogeneous SiO_2 layer is about 2–3 nm (Fig. 3c). The average diameter is about 100 nm for

Table 1
Textural and structural characteristics of samples.

Samples	Textural and structural characteristics		
	Sg_{BET} ($m^2\ g^{-1}$)	Vg_{BJH} ($cm^3\ g^{-1}$)	Dv (nm)
Fe_3O_4	40.9	0.27	26.2
1%SiO_2@Fe_3O_4	83.2	0.31	15.1
3%SiO_2@Fe_3O_4	252.1	0.16	2.5
6%SiO_2@Fe_3O_4	315.5	0.16	2.1
9%SiO_2@Fe_3O_4	266.0	0.17	2.6
10%TiO_2/6%SiO_2@Fe_3O_4	356.3	0.29	2.9
20%TiO_2/6%SiO_2@Fe_3O_4	377.0	0.35	2.7
33%TiO_2/6%SiO_2@Fe_3O_4	420.8	0.35	2.8
50%TiO_2/6%SiO_2@Fe_3O_4	495.3	0.54	3.6
67%TiO_2/6%SiO_2@Fe_3O_4	432.7	0.48	4.5

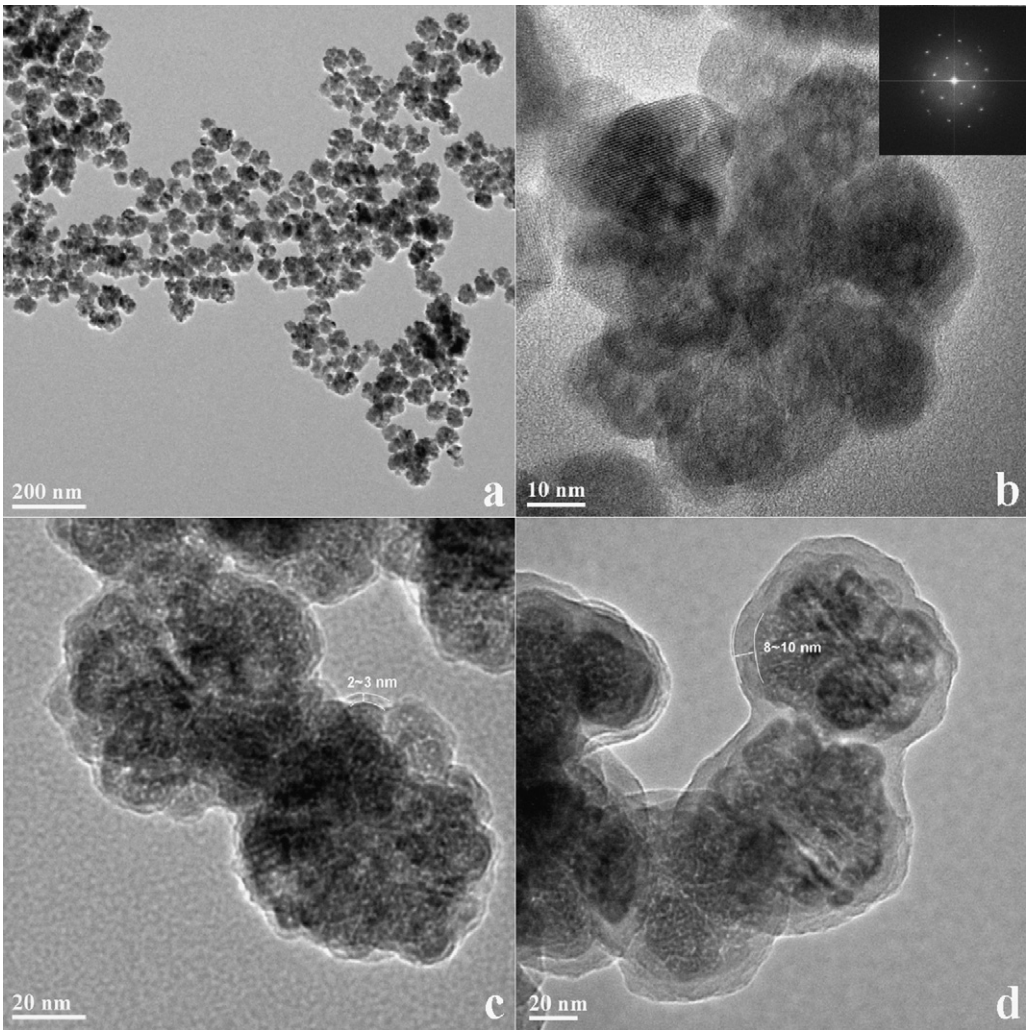

Fig. 3. TEM images of samples: (a and b) Fe_3O_4; (c) 6%SiO_2@Fe_3O_4; (d) 50%TiO_2/6%SiO_2@Fe_3O_4.

the 50%TiO_2/6%SiO_2@Fe_3O_4 microspheres, and the average thickness of the homogeneous anatase TiO_2 layer is about 8–10 nm (Fig. 3d).

Fig. 4 shows the magnetic hysteresis loops of samples. The maximum saturation magnetization of Fe_3O_4, 6%SiO_2@Fe_3O_4 and 50%TiO_2/6%SiO_2@Fe_3O_4 are 83.0 emu/g, 60.5 emu/g and 48.6 emu/g, respectively (Fig. 4a–c). It indicated that all samples had superparamagnetism. The magnetization curve and demagnetization curve are coincidence, no hysteresis phenomenon was found, and remanent magnetization and coercivity are equal to zero. But the hysteresis loops of 6%SiO_2@Fe_3O_4 and 50%TiO_2/6%SiO_2@Fe_3O_4 are weaker than that of Fe_3O_4, it revealed that the coated layers affected the magnetic properties of TiO_2/SiO_2@Fe_3O_4 microspheres. What's more, their maximum saturation magnetization, 60.5 emu/g and 48.6 emu/g (Fig. 4b and c), respectively, are enough strong to preserve their good performance of magnetic recovery [12,20].

3.4. Photocatalytic activity

The relationship curves between TiO_2/SiO_2@Fe_3O_4 catalyst and the photocatalytic performance of RhB aqueous solution are shown in Fig. 5. The SiO_2 content keeps in 6%, as the TiO_2 content from 10% to 33%, the conversion of RhB have been improved from 45% to nearly 98.1%, but it is basically unchanged with the TiO_2 content from 33% to 67% (Fig. 5a). From Fig. 5b, the photocatalytic reaction apparent rate constant (k_a) have the similar trend as the conversion of RhB. In a word, when the 50%TiO_2/6%SiO_2@Fe_3O_4 microspheres are used as catalysts, the conversion of RhB have reached up to 98.1% after 60 min under UV irradiation and the k_a is the maximum. The good photocatalytic activity of 50%TiO_2/6%SiO_2@Fe_3O_4 micspheres may be caused by two factors. One is the small size of the anatase nanocrystals formed during the calcination of the shell, making the TiO_2/SiO_2@Fe_3O_4 microspheres possess high specific surface and mesopore structure, thus they can not only effectively adsorb more molecules and receive more UV light but also offer more reaction sites [21]; another reason is the TiO_2/SiO_2 structure, which has been reported in many papers to show enhancement in the photocatalytic activity [22,23]. In addition, the isolation layer of SiO_2 can prevent electronic interactions between magnetic core and the out layer of TiO_2 [15,16].

Fig. 6 shows the relationship curves between the dosage of 50%TiO_2/6%SiO_2@Fe_3O_4 micspheres and the photocatalytic performance of RhB aqueous solution at the same RhB solution and lighting condition. As 50%TiO_2/6%SiO_2@Fe_3O_4 micspheres from 0.1 g to 0.5 g, all conversion of RhB have been above 98.0% after 60 min under UV light, but adsorption of RhB by catalysts become more and more obvious at the beginning of 30 min (Fig. 6a). Because the quantity of RhB adsorbed by catalysts

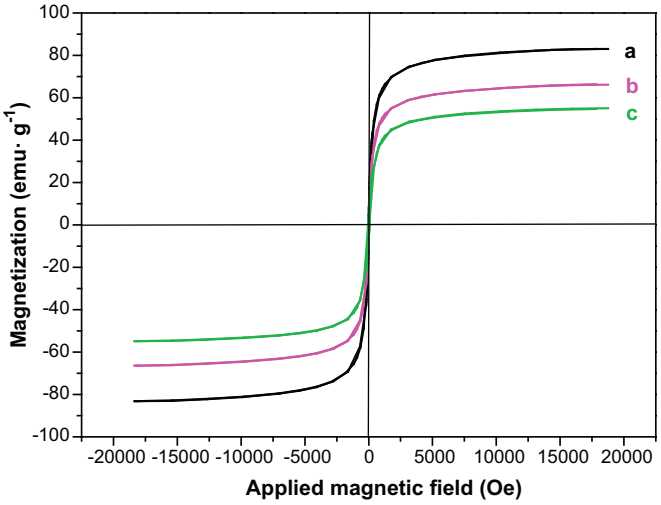

Fig. 4. VSM hysteresis loops of samples: (a) Fe_3O_4; (b) 6%SiO_2@Fe_3O_4; (c) 50%TiO_2/6%SiO_2@Fe_3O_4.

increases with the increasing of catalysts, when the catalysts reach to saturated adsorption, the corresponding solution concentration of RhB is smaller. Noteworthily, the relationship curves of the $\ln C_0/C$ vs. irradiation time are almost straight-line except 0.5 g 50%TiO_2/6%SiO_2@Fe_3O_4 catalyst, and the photocatalytic reaction apparent rate constant $k_a = 0.05288\ min^{-1}$, 0.2 g 50%TiO_2/6%SiO_2@Fe_3O_4 micspheres as photocatalysts, is the maximum (Fig. 6b).

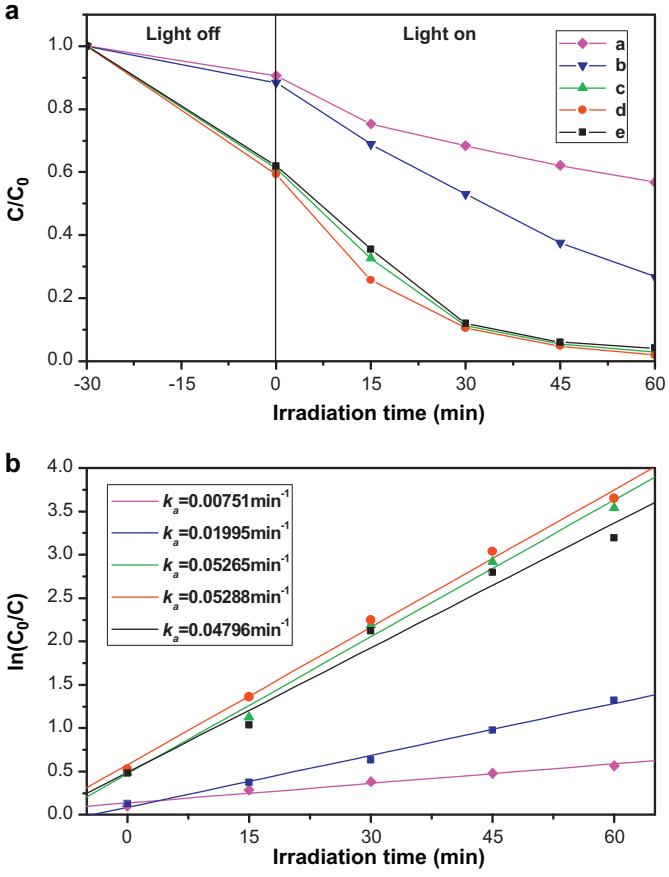

Fig. 5. The relationship curves between TiO_2/SiO_2@Fe_3O_4 catalyst and the photocatalytic performance of RhB aqueous solution: (a) 10%TiO_2/6%SiO_2@Fe_3O_4; (b) 20%TiO_2/6%SiO_2@Fe_3O_4; (c) 33%TiO_2/6%SiO_2@Fe_3O_4; (d) 50%TiO_2/6%SiO_2@Fe_3O_4; (e) 67%TiO_2/6%SiO_2@Fe_3O_4.

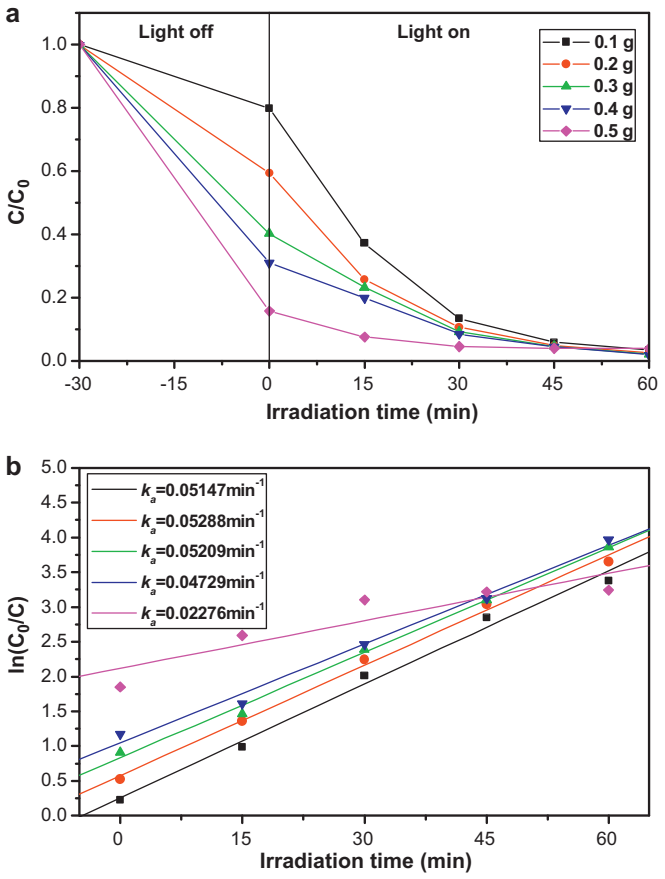

Fig. 6. (a and b) The relationship curves between the amount of 50%TiO_2/6%SiO_2@Fe_3O_4 catalyst and the photocatalytic performance of RhB aqueous solution (200 mL, 10 mg/L RhB aqueous solution).

Fig. 7 shows the relationship curves between the initial concentration of RhB solution and the photocatalytic performance of RhB aqueous solution at the same dosage of 50%TiO_2/6%SiO_2@Fe_3O_4 micspheres and lighting condition. From Fig. 7a, on irradiation of UV light, the concentration of RhB decreases exponentially with the time for every curve. The pseudo-first-order reactions are observed (Fig. 7b) [21]. As the initial concentration of RhB from 10 mg/L to 50 mg/L, the conversion of RhB and the apparent rate constant k_a have apparent decrease. It was well known that the reaction was reactant-limited. The photocatalytic degradation of RhB probably followed the Langmuir–Hinshelwood mechanism. Owing to the fast adsorption process of RhB on the mesoporous TiO_2/SiO_2 structure [23] and the low initial concentration of RhB, the photocatalytic reaction can be described simply by $\ln C_0/C = kKt = k_a t$ [18], where k was the true rate constant which included various parameters, and K was the adsorption constant.

The relationship curves between the reuse time of catalyst and the conversion of RhB are shown in Fig. 8. With the reuse time increasing, the photocatalytic activity of RhB has no obvious decrease. After used for 8 times, the 50%TiO_2/6%SiO_2@Fe_3O_4 catalysts maintain high catalytic activity, and the conversion of RhB decreases by 6% and the quantity loss of catalyst is about 5.0%. It indicated that the 50%TiO_2/6%SiO_2@Fe_3O_4 microspheres had good recycle performance.

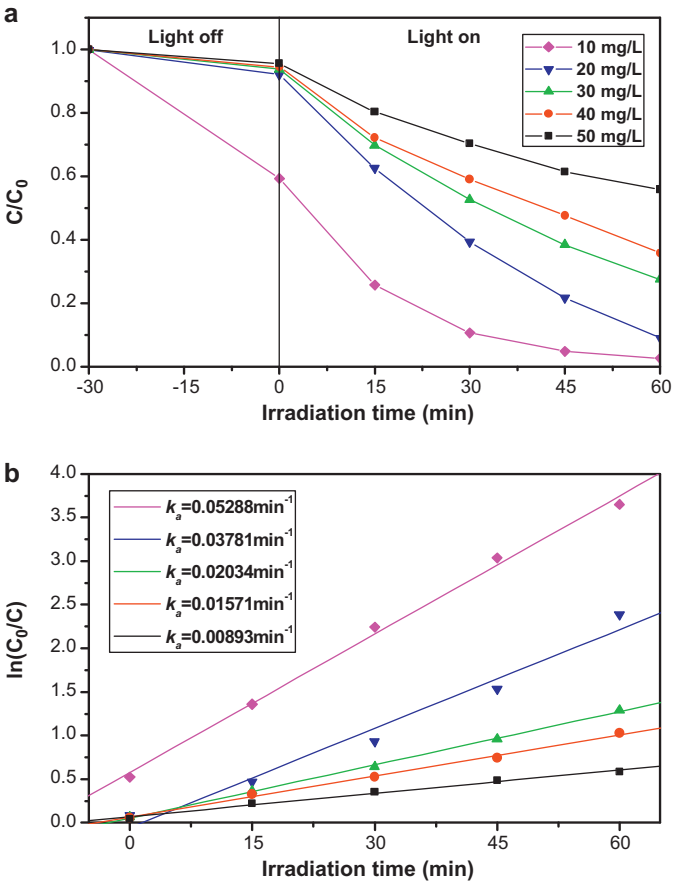

Fig. 7. (a and b) The relationship curves between the initial concentration of RhB solution and the photocatalytic performance of RhB aqueous solution (0.2 g, 50%TiO_2/6%SiO_2@Fe_3O_4 catalyst; 200 mL RhB aqueous solution).

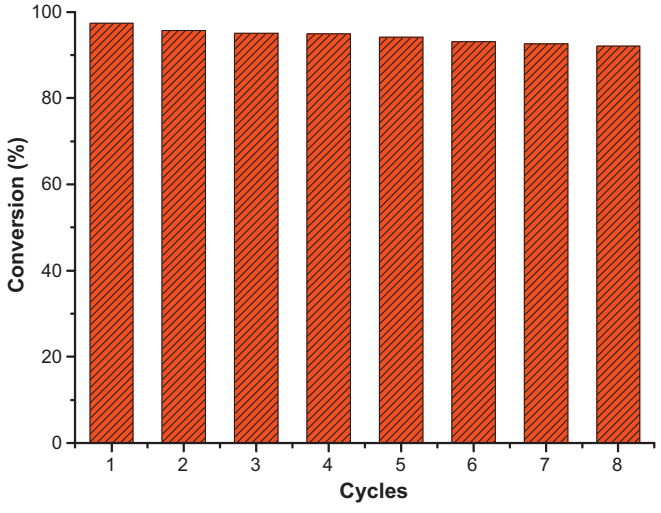

Fig. 8. The relationship curves between the reuse time of catalyst and the conversion of RhB are (0.2 g, 50%TiO_2/6%SiO_2@Fe_3O_4 catalyst; 200 mL, 10 mg/L RhB aqueous solution).

4. Conclusions

Fe_3O_4 particles were successfully synthesized by solvethermal reaction using $FeCl_3$ as reaction substrate, sodium acetate as reducer and ethylene glycol as solvent. The SiO_2@Fe_3O_4 particles were obtained according to the typical Stböer process, and the core-shell TiO_2/SiO_2@Fe_3O_4 microspheres were prepared by sol–gel method. The characterization results showed that the diameter of Fe_3O_4 obtained was about 70 nm, and the thickness of interlayer SiO_2 and outer layer TiO_2 were respectively 2–3 nm and 8–10 nm. In addition, all samples presented high degree of superparamagnetism, and the maximum saturation magnetization of the 50%TiO_2/6%SiO_2@ Fe_3O_4 magnetic microspheres still kept at 48.6 emu/g. The BET surface area of the 50%TiO_2/6%SiO_2@ Fe_3O_4 magnetic microspheres reached up to 495.3 m^2/g. The catalytic performance for the photocatalytic degradation of RhB was researched under UV irradiation. When the contents of SiO_2 and TiO_2 were respectively 6% and 50%, the catalyst exhibited the best photocatalytic activity, and the conversion of RhB can achieve up to 98.1%. The photocatalytic reaction apparent rate constant k_a was 0.05288 min^{-1}. After used 8 cycles, the prepared TiO_2/SiO_2@Fe_3O_4 catalysts also maintained high photocatalytic activity and catalyst recovery.

Acknowledgement

Financial funds from the National Natural Science Foundation of China (project 20473009) are gratefully acknowledged.

References

[1] S. Malato, P. Fernández-Ibañez, M.I. Maldonado, J. Blanco, W. Gernjak, Catal. Today 141 (2009) 1–59.
[2] J. Wang, R.H. Li, Z.H. Zhang, W. Sun, Y.P. Xie, R. Xu, Z.Q. Xing, X.D. Zhang, Environ. Prog. 27 (2008) 242–249.
[3] Z.Z. Zhang, X.X. Wang, J.L. Long, Z.X. Ding, X.L. Fu, X.Z. Fu, Appl. Catal. A 380 (2010) 178–184.
[4] U.G. Akpan, B.H. Hameed, J. Hazard. Mater. 170 (2009) 520–529.
[5] J.M. Herrmann, Catal. Today 53 (1999) 115–129.
[6] X. Chen, C.W. Li, J. Wang, J. Li, X.Y. Luan, Y. Li, R. Xu, B.X. Wang, Mater. Lett. 64 (2010) 1437–1440.
[7] J.A. Byrne, B.R. Eggins, N.M.D. Brown, B. McKinney, M. Rouse, Appl. Catal. B 17 (1998) 25–36.
[8] A. Haarstrick, O.M. Kut, E. Heinzle, Environ. Sci. Technol. 30 (1996) 817–824.
[9] A. Tarek, G. Allah, K. Fujimura, S. Kato, S. Satokawa, T. Kojima, J. Hazard. Mater. 154 (2008) 572–577.
[10] S.W. Lee, J. Drwiega, C.Y. Wu, D. Mazyck, W.M. Sigmund, Chem. Mater. 16 (2004) 1160–1164.
[11] Q.H. He, Z.X. Zhang, J.W. Xiong, Y.Y. Xiong, H. Xiao, Opt. Mater. 31 (2008) 380–384.
[12] S.H. Xuan, W.Q. Jiang, X.L. Gong, Y. Hu, Z.Y. Chen, J. Phys. Chem. C 113 (2009) 553–558.
[13] Y. Gao, B.H. Chen, H.L. Li, Y.X. Ma, Mater. Chem. Phys. 80 (2003) 348–355.
[14] V. Belessi, D. Lambropoulou, I. Konstantinou, R. Zboril, J. Tucek, D. Jancik, T. Albanis, D. Petridis, Appl. Catal. B 87 (2009) 181–189.
[15] D. Beydoun, R. Amal, G. Low, S. McEvoy, J. Mol. Catal. A: Chem. 180 (2002) 193–200.
[16] D. Beydoun, R. Amal, G.K.C. Low, S. Mcevoy, J. Phys. Chem. B 104 (2000) 4387–4396.
[17] Y.H. Deng, D.W. Qi, C.H. Deng, X.M. Zhang, D.Y. Zhao, J. Am. Chem. Soc. 130 (2008) 28–29.
[18] J.C. Yu, J.G. Yu, J.C. Zhao, Appl. Catal. B 36 (2002) 31–43.
[19] J.J. Xu, Y.H. Ao, D.G. Fu, C.W. Yuan, J. Phys. Chem. Solids 69 (2008) 1980–1984.
[20] Y.F. Zhu, W.R. Zhao, H.R. Chen, J.L. Shi, J. Phys. Chem. C 111 (2007) 5281–5285.
[21] M.M. Ye, Q. Zhang, Y.X. Hu, J.P. Ge, Z.D. Lu, L. He, Z.L. Chen, Y.D. Yin, Chem. Eur. J. 16 (2010) 6243–6250.
[22] X.Z. Fu, L.A. Clark, Q. Yang, M.A. Anderson, Environ. Sci. Technol. 30 (1996) 647–653.
[23] W.Y. Dong, C.W. Lee, X.C. Lu, Y.J. Sun, W.M. Hua, G.S. Zhuang, S.C. Zhang, J.M. Chen, H.Q. Hou, D.Y. Zhao, Appl. Catal. B 95 (2010) 197–207.